HYDROVOLCANISM IN OKMOK CALDERA, ALASKA

By

Leslie Deanne Almberg

RECOMMENDED:

David Lescinsky

Advisory Committee Chair

Chair, Department of Geology and Geophysics

APPROVED:

Dean, College of Science, Engineering and Mathematics

Dean of the Graduate School

December 8, 2003

Date

HYDROVOLCANISM IN OKMOK CALDERA, ALASKA

A

THESIS

Presented to the Faculty

of the University of Alaska Fairbanks

in partial Fulfillment of the Requirements

for the Degree of

MASTER OF SCIENCE

By

LESLIE DEANNE ALMBERG, B.S.

Fairbanks, Alaska

December 2003

ABSTRACT

Hydrovolcanic activity in Okmok Caldera predominated on the crater floor during approximately the first 775 years after the caldera collapsed at 2050 yr. B.P. Interactions between rising magma and shallow water (<100 m) controlled the development of lithofacies observed in the early post-caldera deposits. The distinctive lithofacies reflect the eruptive processes active as Cone D, a composite tuff, lava flow, and cinder cone, breached the surface of a lake which once covered the caldera floor. Three phases of eruptive activity constructed Cone D: first, a subaqueous cycle; second, emergent; and finally a purely subaerial strombolian and hawaiian phase built the edifice to its current height.

Radiocarbon dates provide constraining ages for a catastrophic flood that emptied the 4.3×10^9 m^3 caldera lake and exposed the subaqueous lithofacies. An effusion rate of 2.7×10^6 m^3yr^{-1} for this early eruptive period is calculated using eruptive volumes determined from a 5-m resolution DEM, based on AirSAR data. The prehistoric effusion rate determined for Cone D is on the same order of magnitude as the calculated historic effusion rate of $\sim 5.3 \times 10^6$ m^3yr^{-1} from Cone A, based on mapped extents and thicknesses of lava flows and the cone itself.

TABLE OF CONTENTS

LIST OF FIGURES

LIST OF TABLES

LIST OF APPENDICES

ACKNOWLEDGEMENTS

I would like to thank Jim Begét for suggesting this field site, working and learning with me in the caldera, and providing the funding and support to make this project possible. I am very grateful and deeply indebted to Tina Neal for her incredible cheerleading of my efforts, numerous edits of this and other written works, brainstorming sessions, loan of samples, descriptions of deposits, and all-around moral support. To Dave Lescinsky, I offer a resounding "thank you" for the time and effort invested in teaching me how to recognize and describe lava fracture patterns, for the lively banter and base camp expertise in the caldera, for picking me up every time I fell, and for the wonderful set of photos to work with. I would also like to thank Jess Larsen for sticking out the field season with us, in spite of major set backs, pushing me when I needed it, and not being afraid to explore wild ideas on the fly. And without Janet Schaefer, I could have made no volume calculations and my figures would have been flat.

Additionally, I would like to thank: Anthony Arendt for assimilating the Dutch Harbor climate data and his editorial comments; Chris Nye for rescuing me from the death march, reminding me not to completely lose my sense of humor in the field, "finding" Surtsey for me, and the use of his digital photographs; Claude Duguay for helping me to learn PCI Geomatica; Bill Witte for being quick to respond to computer emergencies; Norma Pfeiffer for answering my never-ending list of questions concerning my degree program; Rainer Newberry and Mary Keskinen for their indispensable help; Amanda Kolker for all of the wonderful lunches; and AVO for allowing me to be a part of their research efforts in the Aleutians.

CHAPTER 1: INTRODUCTION

Okmok, a basaltic andesite shield volcano, is situated on the northeastern half of Umnak Island in the eastern Aleutian Islands (Fig. 1.1). Okmok is built upon Tertiary volcanic rocks and has a 10 km wide central caldera. Extensive evidence exists for caldera-forming events at c.a. 12,000 yr. B.P. and 2050 yr. B.P. (Begét, unpublished data; Wolfe and Begét, 2003), including concentric caldera walls along the northern rim and lava flows, pyroclastic fall deposits, and erosional features between two massive ignimbrite sheets (Byers, 1959; J. Begét, pers. comm.; Larsen and Nye, 2003; Larsen, 2003).

The caldera has been partially refilled since the 2050 yr. B.P. caldera collapse by numerous tuff rings and cones, cinder cones, and lava flows. Byers and others (1947) identified ten vents, distributed primarily along two arcuate zones, and assigned them letters A through J based on an interpretation of their relative age, with Cone A being currently active (Fig. 1.2). Age relations were based on degree of dissection, eruptive style, and accessory minerals present in lavas. The relative ages were re-interpreted by Byers in subsequent publications (1959) and an ongoing mapping project in the caldera is further refining the age of these features. Byers (1959) first noted the presence of both subaerially and subaqueously erupted volcaniclastics and lava flows within the caldera.

Cone D, the focus of this study, is a relatively small (0.59 km^3) but complex lava, cinder, and tuff cone in Okmok Caldera (Appendix A). The shape of Cone D is unique - the edifice is composed of a cinder cone, at the angle of repose, rising above a broad, flat bench. The bench is composed primarily of thin (~2 m) pahoehoe flow deltas. The cliff edges are lined with bifurcating lava tubes that spill over the cliff edge at angles of 20-45° on the side of the cone facing the caldera center. The maximum cliff height is ~100 m. This morphology is similar to landforms formed by two disparate processes: tuyas, created through confinement of eruptive products within an englacial vault (Hickson,

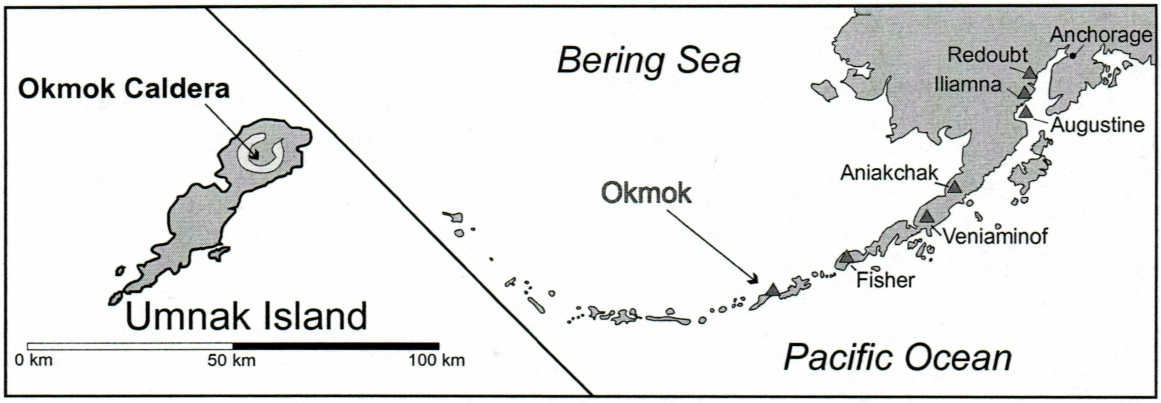

Fig. 1.1 Location map of Okmok Caldera. The caldera occupies the northeastern half of Umnak Island, in the eastern Aleutian Islands of southwestern Alaska. A few of the other active volcanoes along the Aleutian Arc and the city of Anchorage are marked for reference.

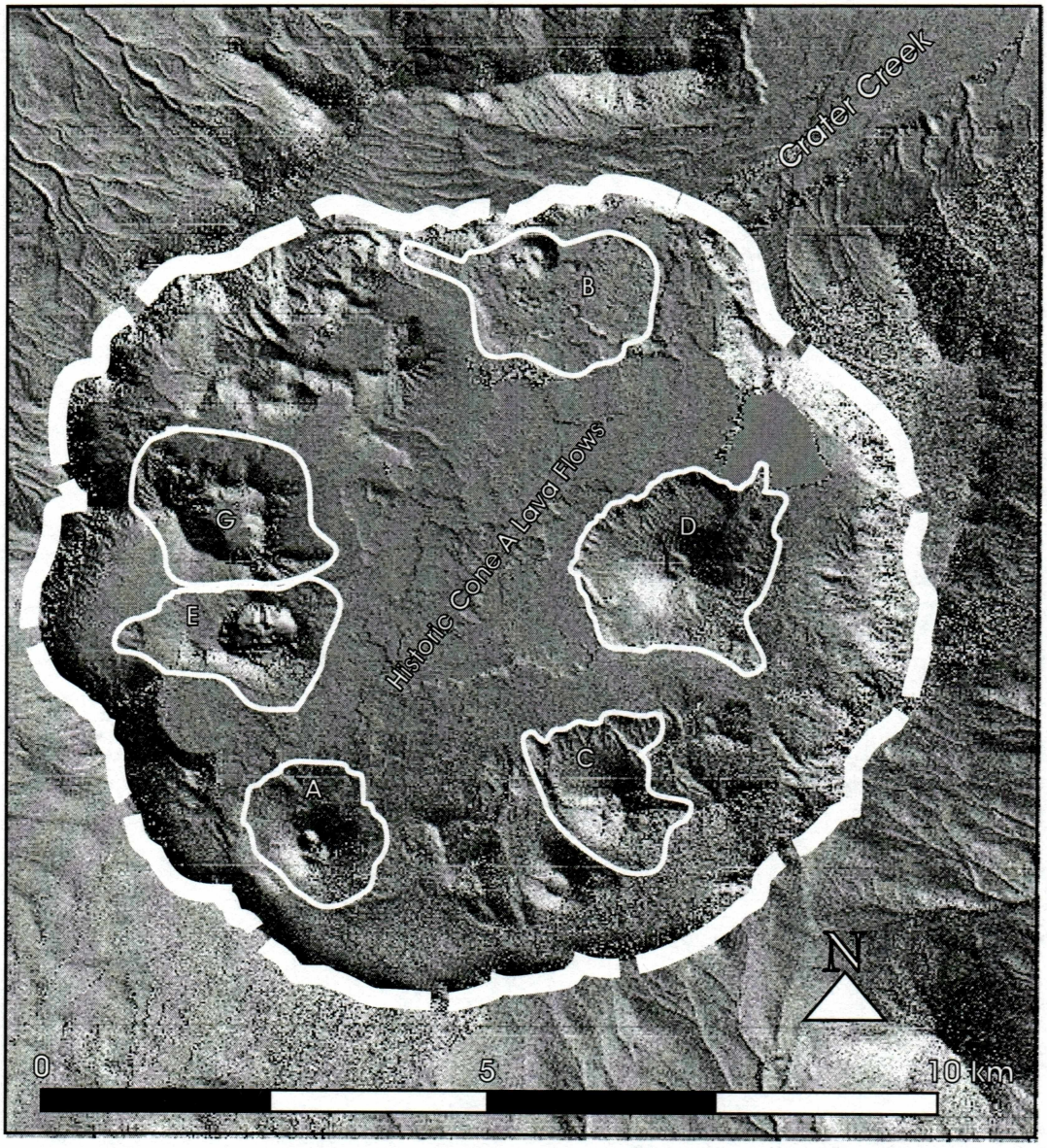

Fig. 1.2 Major features of Okmok Caldera discussed in the text. Base map is from a 5-m resolution DEM generated from AirSAR data from the Alaska SAR Facility. The dashed white line indicates the caldera rim formed during the 2050 y.b.p. ignimbrite-forming eruption. Thin white outlines delineate approximate boundaries of intra-caldera cones as named by Byers and others (1947).

2000); and cones developed concurrently with rising lake water (Bacon et. al., 2002). There is little evidence to suggest the presence of a caldera-filling glacier after the 2050 yr. B.P. eruption, although moraines and glacial deposits indicate small glaciers were once more extensive (Byers, 1959). Deltas, shorelines and lacustrine sediments, however, record the presence of a ~150 m deep lake (Byers 1959, Wolfe and Begét, 2003).

The record of subaqueous volcanism at Okmok Caldera is unusual because draining of the caldera lake has exposed all of Cone D, allowing us to observe almost the complete volcanic sequence. The relatively young age of this edifice and its extensive exposure provide a useful comparison to the deeply eroded emergent cones in the geologic record and to the more limited studies of subaerial deposits observable at modern sites of hydrovolcanism. The presence of an early post-caldera lake and a sequence of changing vent conditions are recorded in the deposits from Cone D. The eruptive products related to Cone D reveal a shallowing upward sequence, indicating that the edifice was growing faster than the lake was rising

Cones C and D are broadly similar in their morphology. Both consist of symmetrical cinder cones perched atop broad, flat benches of subaerially effusive lavas. Cone C appears to be superimposed over a tuff cone with a separate vent on its southern side, whereas Cone D's caldera wall side consists of truncated lava flows, with little to no talus below steep cliffs, unconsolidated hydrovolcaniclastic material, and reworked colluvial sediments. The cones' summit regions are also different: Cone C has multiple craters, with hot, active fumaroles (~95°C, Byers, 1959; 87-110°C, K. Papp, unpubl. data), whereas Cone D has a single crater, exposing a vent plug of crystalline basalt (Byers, 1959).

Young (<200 a) lava flows from Cone A, cover most of the caldera floor. The 1945 eruption was the first observed by U.S. Geologic Survey volcanologists (Byers et. al., 1947). Subsequent activity at Cone A produced lava flows in 1958 and 1997 (Miller

et. al., 1998) and built up a tephra pile around the vent. Byers and others (1947) noted that a pre-1945 flow from Cone A was not covered with any ash or vegetation, and inferred that it had been erupted within the preceding few decades.

Byers (1959) described lake sediments covering much of the caldera floor. These were largely buried by the 1958 lava flow, and only a few varve-like deposits remain exposed along the banks of Crater Creek before it exits the caldera, and on the benches of Cones C and D. Wolfe (2001) estimated that the maximum volume attained by the lake was 5.8×10^9 m^3, from a simple cylinder model using the maximum lake extent within the caldera and an average depth. At the lake's highest stand, water-laid sediments were deposited on the benches of Cones C and D and etched a sharp slope break around the base of Cone D's cinder pile, indicating that activity from this vent ceased before the lake drained between 1560 and 1010 yr. B.P.

Wolfe (2001) found evidence for two catastrophic flooding events on the plains of Crater Creek. This is consistent with Byers observation of wave-cut terraces below the bench of Cone D, indicating that the lake partially refilled after the first major flood. Radiocarbon dates for the flood events (Wolfe and Begét, 2003) give constraining ages for emptying of the caldera lake. This event is also recorded in sediments overlying Cone D.

Observations of hydrovolcanic products have been made both in and out of the caldera (e.g. Wong, 2002; Neal et. al., 2003; Wolfe and Begét, 2003). Byers and others (1947) first suggested that Cones C and D were erupted through the lake that filled Okmok's crater. Surge deposits up to 10 m thick are found at several localities on the flanks of Okmok (Wolfe, 2001; J. Begét, pers. comm.; A. Burgisser, pers. comm.) and more than 2 m thick on the upper bench of Cone D, indicating that multiple high-energy eruptions breached the caldera lake during its ephemeral existence. Because of the

homogeneity of post-caldera products, it would be difficult, if not impossible, to distinguish the vent from which each surge came.

Hydrovolcanism has been significant at Okmok throughout its eruptive history. The eruptive processes controlled by the interaction of magma and water produced many of the products seen in the stratigraphic sequences both within and without the caldera. Therefore I utilize the distinctive characteristics of such products to develop a model for development of Cone D.

I find extensive evidence for magma/water interaction within the deposits of Cone D. "Wet" features, such as accretionary lapilli, bomb sags, and pseudopillows indicate that magmatic products encountered water before solidifying. By comparing the stratigraphic relationships of such deposits with "dry" features (juvenile cinders, basaltic spatter, and pahoehoe flows), I develop a model for the growth of Cone D through the extinct crater lake, which once filled much of Okmok Caldera. My interpretations of these stratigraphic relationships are based on observations of hydrovolcanic activity and deposits at active volcanic centers, as described in previous studies (Kokelaar and Durant, 1983; Jakobsson and Moore, 1986; Houghton and Smith, 1993; Morrissey et. al., 2000), experimental work (Wohletz, 1986; Kokelaar, 1986), and deposits in the geologic record (Wohletz and Sheridan, 1983; Cas et. al., 1989; Godchaux et. al., 1992; Orton, 1996; White 1996; White, 2001).

CHAPTER 2: METHODS

2.1 Field Methods

Fieldwork was carried out at Okmok Volcano from July 31 to August 17, 2003. Work was done on foot from a field camp in the caldera during the first week and, weather permitting, with the aid of a helicopter based at Fort Glenn in the subsequent weeks. All funding for field support was provided as part of an ongoing effort by the Alaska Volcano Observatory (AVO) to re-map and re-interpret the caldera geology.

Conventional field methods were employed for sampling and mapping within the caldera. We[1] first made reconnaissance trips on foot around both Cone D and Cone C to get a general idea of the geological layout and determine which areas should receive more focused scrutiny. More time was later spent at geologically interesting outcrops, but the number of sites was restricted by inclement weather. Mapping was done on 1-m spatial resolution IKONOS satellite images, acquired July 3, 2002 and September 15, 2000.

On the well-defined southwestern lava delta of Cone D, we made numerous measurements detailing the characteristics of the bench lavas (see Table 3.4). We measured the strike and dip of lava tubes by sighting a Brunton transit compass down the center of each identifiable tube and measuring the average dip angle. The width, length, and height of each tube were measured to the closest approximation of where the tube began and ended. Erosion and development of soils occasionally obscured the edges of lava tubes, increasing the error in measurements. We made these measurements only around the northwest half of the lava delta as the character of the

---

[1] Professors James E. Begét and David T. Lescinsky assisted me in the field.

lava flows changed and the cliffs appeared to have collapsed elsewhere, so it was no longer possible to make such measurements.

In the field we identified phenocrysts and estimated vesicularities from hand specimens. We distinguished eight units within the sequence of volcanic products comprising Cone D based on their characteristics and spatial relationships. Using a hand-held GPS unit we recorded varying water levels where lavas entered the paleo-lake after flowing across the bench. The lava bench height was determined from a 10-m topographic map of the caldera created from AirSAR elevation data.

It was possible to glean further information about Cone D units, and their correlation to other cones within the caldera from photographs taken on many helicopter flights in the caldera. The observations and samples of other AVO geologists, collected as part of the caldera re-mapping project, were also incorporated into this research.

I constrained the timeline for the effusion of Cone D products in three steps. First, Cone D could not have been built prior to the 2050 yr. B.P. caldera collapse, thus this is the lower bounding date for onset of activity at this vent. Second, the sharp slope break around the base of Cone D's cinder pile indicates that activity at this vent shut off while the paleo-lake was still present. This hypothesis is further supported by the presence of lacustrine sediments on the upper bench of Cone D. Therefore the date of the catastrophic caldera-draining flood, determined by radiocarbon dating of organic soils by Wolfe and Begét (2003), provides the upper boundary for effusion at Cone D.

2.2 Analytical Methods

Volume calculations of Cones C and D deposits, older tuff cones, and the caldera-filling lake were made using PCI Geomatica™, a geographic information system

(GIS) package. I resampled high-resolution (5 m) digital elevation model (DEM) created from synthetic aperture radar (AirSAR) data, from the Alaska SAR Facility, using the nearest neighbor smoothing algorithm. This corrected for incorrect data points, which commonly occurred in areas of high aspect ratio or that had snow or water cover at the time of the image acquisition. Some values were manually corrected in areas of interest where ground truth elevations were determined using a hand-held GPS unit.

Masks of each region of interest (individual cones, lake area, etc.) were created to allow for the calculation of irregular areas and volumes. The volume calculation algorithm in PCI Geomatica™ uses the area of the mask and the distance from a selected elevation up or down to a surface set by the DEM at each point to determine positive, negative, net and total volumes (Fig. 2.2). I chose elevation values for each calculation based on GPS elevation data collected at stratigraphic markers in the field. This method assumes a horizontal base for each deposit and does not take into account eruptive products that were ejected from the caldera.

For younger flows, areas were calculated using SCION Image from USGS maps of the caldera floor. Volumes were computed using the average thickness of flows, as reported by workers in the caldera, in conjunction with the flow area.

I used standard petrographic methods to identify calcite within thin sections of samples from Duh. I further distinguished between samples with and without calcite using a dilute solution of HCl.

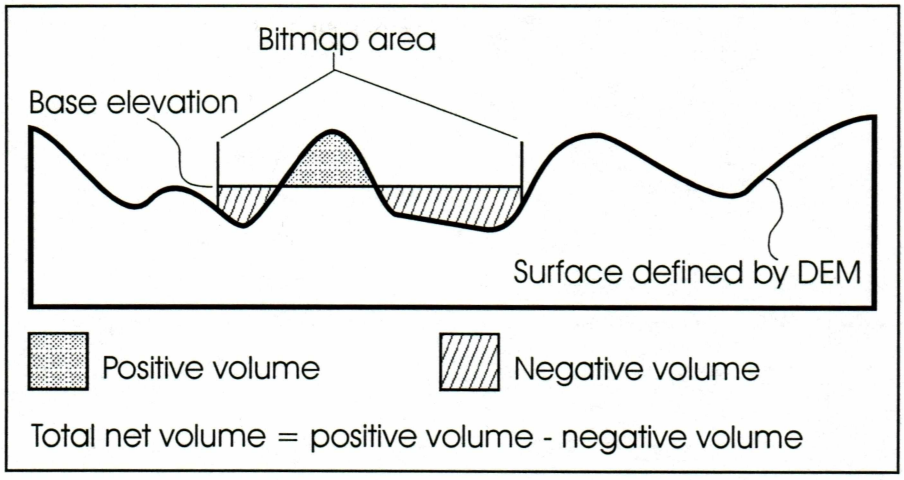

Fig. 2.2 Cartoon illustrating volume calculation function used in PCI Geomatica. The bitmap area and base elevation are user defined to select the three dimensional region of interest. A distance down from the base elevation to the DEM surface is considered negative, whereas a distance up is considered positive. The program returns calculations of positive volume, negative volume, total net volume, and total absolute volume = positive volume + negative volume, based on user defined parameters and the DEM surface.

CHAPTER 3: DEPOSIT DESCRIPTIONS AND INTERPRETATIONS

3.1 Lower Hyalotuff (Dlh)

Description – Lowest most unit comprised of more than 15 m of massive, weakly consolidated, ash to bomb size fragments of dense black scoria with conspicuous white plagioclase crystals (1-2 mm). In two localities, the unit was welded and displayed polygonal cooling joints and chilled surfaces with what appear to be drip features. Vesicularity in juvenile material is weak to absent, with 0.1-4 mm irregular vesicles clustered in concentric bands. Repeated horizons of lapilli and blocks, defined by sharp changes in grain size and coarse tail grading, with no definite bedding planes (pseudo-beds), dip away from the vent (Fig. 3.1.1). Orientation of pseudo-beds varies abruptly and dramatically within a few meter section. Rootless fumaroles break unconformably through the overlying strata of Cone D Upper Hyalotuff (Duh) and are surrounded by areas of alteration (Fig. 3.1.2). Small (<20 cm) lava pillows and pillow fragments, in a matrix of palagonitized ash, are present near some fumaroles.

This unit underlies all other exposed units described in this text. It is exposed only in the northern-most section of Cone D deposits, along the lakeshore. Duh deposits overlie it unconformably (Appendix A).

Interpretation – Hot juvenile material, of constant composition, appears to have erupted below lake level and been carried by gravity flow away from the vent region during the first eruptive phase from the proto-Cone D vent as suggested by the coarse tail grading and abrupt variations in bedding orientation (c.f., White, 1996). Cyclic variations in grain size result from subaqueous explosions and collapsing jets. The small, rapid fluctuations in dip direction and orientation, grain size, and bedding thickness result from changes in the mechanical energy available from water/magma mixing and the tephra jet trajectory (Wholetz and Sheridan, 1983). The erupting magma appears to have

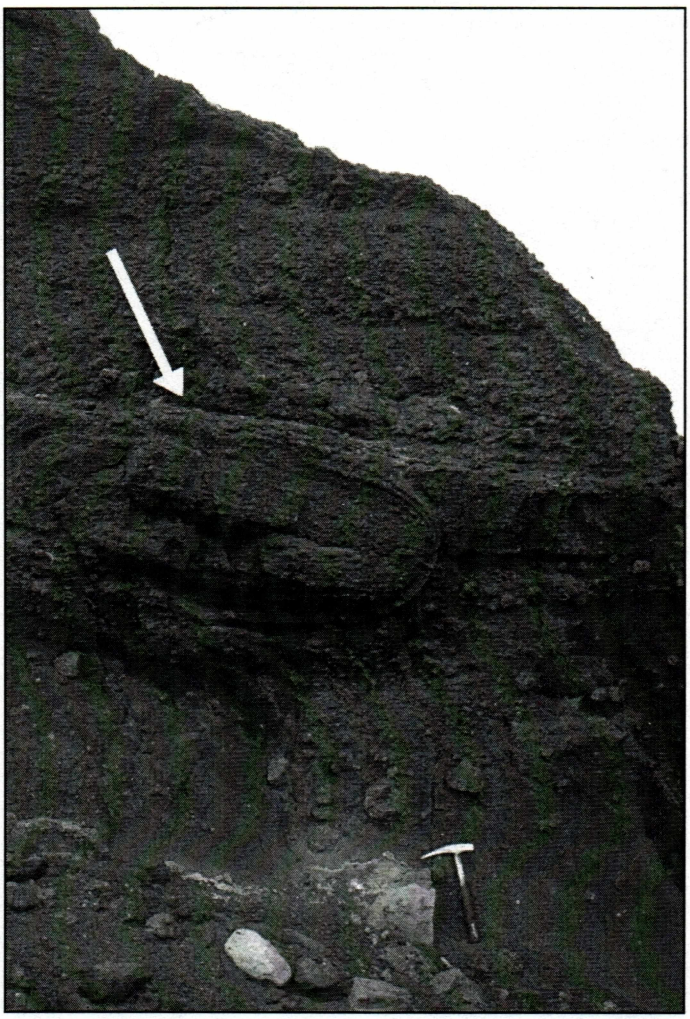

Photo by D.T. Lescinsky, UWO

Fig. 3.1.1 Pseudo bedding and normal grading are displayed within unit Dlh. Feature in photo center (arrow) was formed by gravity flow of dilute slurry away from the vent (left of photo). Rock hammer is approximately 35 cm.

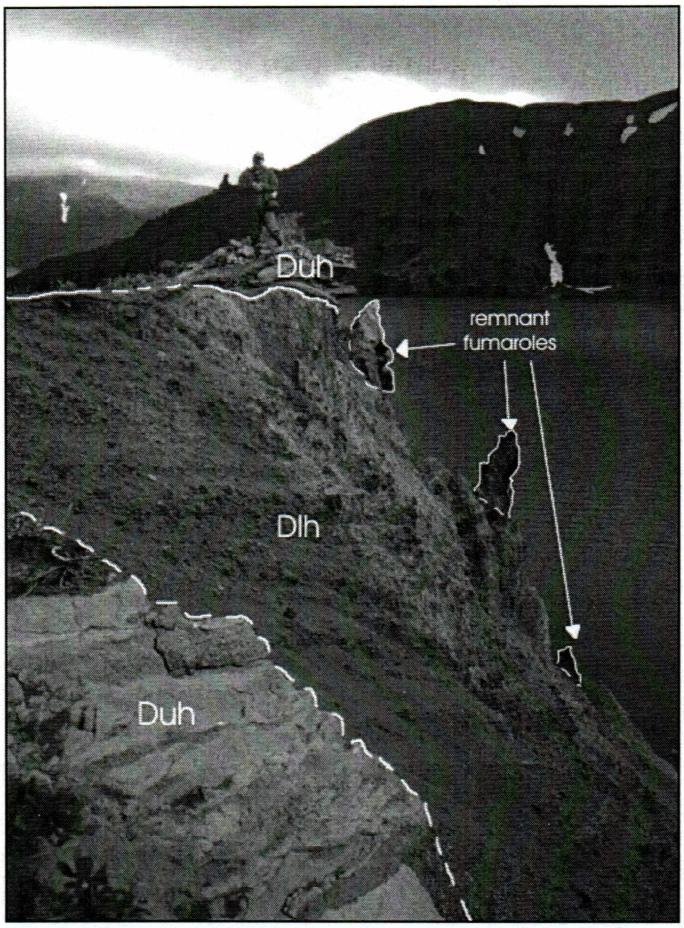

Fig. 3.1.2 Professor J.E. Begét stands above the unconformable contact of Dlh and Duh. The remnant fumaroles, which break through the overlying beds of Duh (to left of scene), are evidence for incipient boiling of water as Dlh was emplaced, indicating that the deposit was hotter than 100°C and water saturated as Duh was deposited.

been mostly degassed during this eruptive phase, indicated by the sparse vesicles. The paucity of vesicles indicates that explosive energy must have resulted from contact between relatively cold lake water and magma.

3.2 Upper Hyalotuff (Duh)

Description – A cliff-forming unit composed of >50-100 layers, each 30-130 cm thick, of well indurated, planar beds composed of fine-grained yellowish/buff ash and lapilli, alternating repeatedly with beds of sub rounded to sub angular, coarse (~5 cm) dense to poorly vesicular juvenile clasts with conspicuous plagioclase crystals (characteristic of Cone D eruptive products) (Fig. 3.2.1) is present on the eastern side of Cone D. Finer-grained beds support abundant plant growth due to water retention of clay minerals. Some layers consist primarily of large clasts, with bombs and bomb sags present (Fig. 3.2.2). The top layer has coarse (20-30 cm) angular blocks of lithics plus blocks of excavated palagonite up to 0.5 m. Below this top coarse-grained layer, layers are typically finer-grained than lower in the section, with more altered yellow matrix. Interstitial calcite is present in the lowest occurrence of this unit.

Dip angles range from 18-37°, striking northeast, and vary randomly throughout the section. Several faults cutting through the outcrop at various angles offset beds by as much as 1 m. Only minor amounts of talus exist below the 60 m cliff. A >7 m thick, southeast striking, block of the same unit, apparently *in situ*, is located 380 meters to the east with shallower dip angles.

Another outcrop of Duh displays characteristics that differ from the two other outcrops. The 20-30 cm of material discordantly mantling Dlh is composed of 3-5 cm well-indurated beds with complex changes in dip direction. Abundant accretionary lapilli are present, along with gray-brown to black, plagioclase rich lithics, in a pebbly to

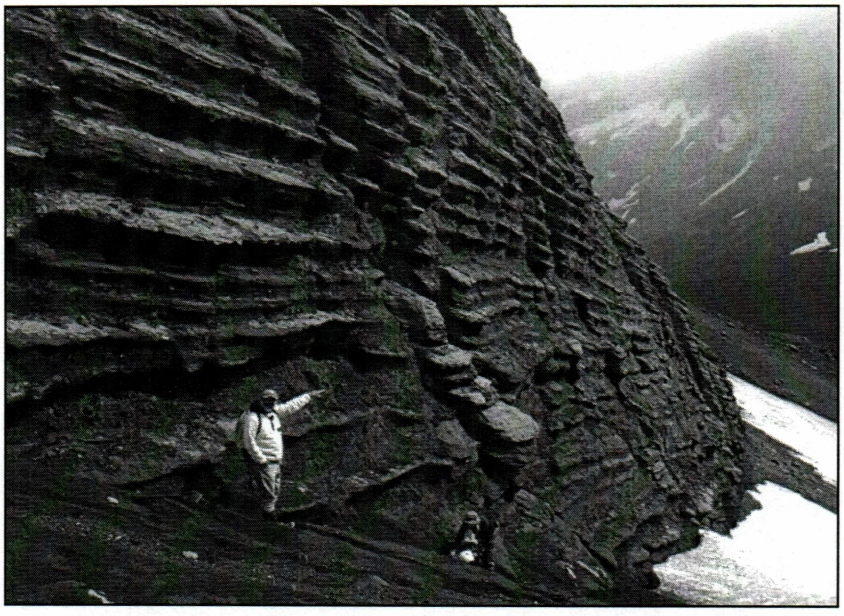

Photo by D.T. Lescinsky, UWO

Fig. 3.2.1 Repeated bedding pattern within unit Duh. Dr. James E. Begét points out this phenomenon in the cliff-forming unit, resulting from fluctuations in explosivity.

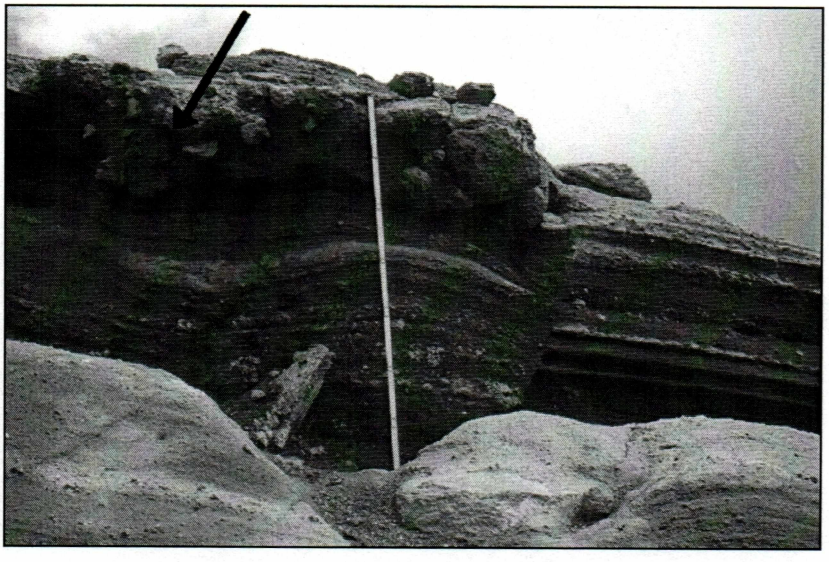

Photo by D.T. Lescinsky, UWO

Fig. 3.2.2 Bomb sag seen in the upper beds of Duh. Stick is 1 m.

fine ash matrix. Rootless fumaroles of Dlh material brittlely deform the beds upward at three localities.

This deposit is exposed only in the eastern half of Cone D. Outcrops jut out unconformably from the cinder pile (Dcc) and arms of unconsolidated volcaniclastics (Duv) as illustrated in Appendix A. Although outcrops of this deposit are found at higher elevations than other units, its relationship to the underlying Dlh deposits place it lower in the stratigraphic sequence.

Interpretation – More explosive energy than was acting during the formation of Dlh is required for such extensive comminution of the bulk of the material ejected during this second eruptive phase (Kokelaar and Durant, 1983). The explosivity appears to be cyclical, suggesting rapid drying of the vent during each discrete eruption, with enough time between eruptions for re-flooding of the vent. The lowest occurrence of this unit was likely deposited in water (resulting in the presence of calcite) (Godchaux et. al., 1992) but may have traveled subaerially before coming to rest, resulting in the formation of accretionary lapilli.

The thickest deposit of this unit likely comprised part of a tuff cone crater rim while an earlier vent was active. The thickness of the deposit, steep maximum bedding dips, high degree of induration and palagonitization, and bedding thickness are all consistent with observations of tuff cones elsewhere (Wholetz and Sheridan, 1983). A shallow depression on the east side of Cone D, adjacent to the outcrop of Duh (blue dashed circle in Appendix A), is inferred as the vent for these deposits.

3.3 Unconsolidated Volcaniclastics (Duv)

Description – Two steep-sided parallel ridges of unconsolidated, juvenile ash and scoria with occasional non-juvenile lithics radiate out from the NE side of the cone (Fig. 3.3,

Fig. 3.3 Parallel ridges of unconsolidated volcaniclastic material radiating out to the northeast of Cone D. Large snow patch in photo center is ~40 m wide.

Appendix A). No apparent bedding was noted. Colluvium from Cone D overlies these deposits at about 540 m ASL.

Interpretation – The volcaniclastics were produced synchronously with Duh deposits in the same manner as the tuff cones elsewhere in the caldera and then reshaped by the erosional power of the lake water as it catastrophically exited the caldera. Tephra jetting, analogous to that seen at Surtsey (Iceland), Ta'al (Philippines) and Capelinhos (Azores) (Thorarinsson, 1964; Waters and Fisher, 1971), would have dispersed pyroclasts radially from the vent, with the vent at or near water level. Without the armoring of lava flows that protected the western half of the cone, these deposits would have been more susceptible to erosion and reworking, obscuring original bedding and spatial relationships to other units.

3.4 Youngest Bench Lavas (Dbl)

Description – Ropy, black to dark gray, mainly pahoehoe basalt flows, dipping 5-15°, bifurcate near the cliff edges forming three distinct lava deltas in the northwest and southwest quadrants of Cone D (Fig. 3.4.1, Appendix A – outlined in heavy dotted lines). These lava deltas are distinguishable in the IKONOS image of Cone D. Where lava deltas form, individual flows are thin (1-2 m) and the bench edge is distinct. To the east of the cone (facing the caldera wall), flows are thicker (3-5 m), sporadically distributed, delta formation is not apparent, and flows terminate abruptly without flowing over a cliff edge. Lava deltas to the north and west of Cone D are more eroded and have thicker soil horizons. Some lava deltas have cliffs too steep for safe working conditions.

The data set we amassed from the southern lava delta on Cone D details changes in the lavas where they flow over the cliff edge after traveling across the bench surface. The lava tube measurements we collected (Tables 3.4.1 and 3.4.2) define a radial pattern

Fig. 3.4.1 Ropy textures of subaerially erupted pahoehoe lavas forming the bench of Cone D are accentuated here in black. Steaming in the background results from rainwater boiling on the still cooling 1997 lava flow. Lava block sitting on flow is of unknown origin. Field book is 18 cm.

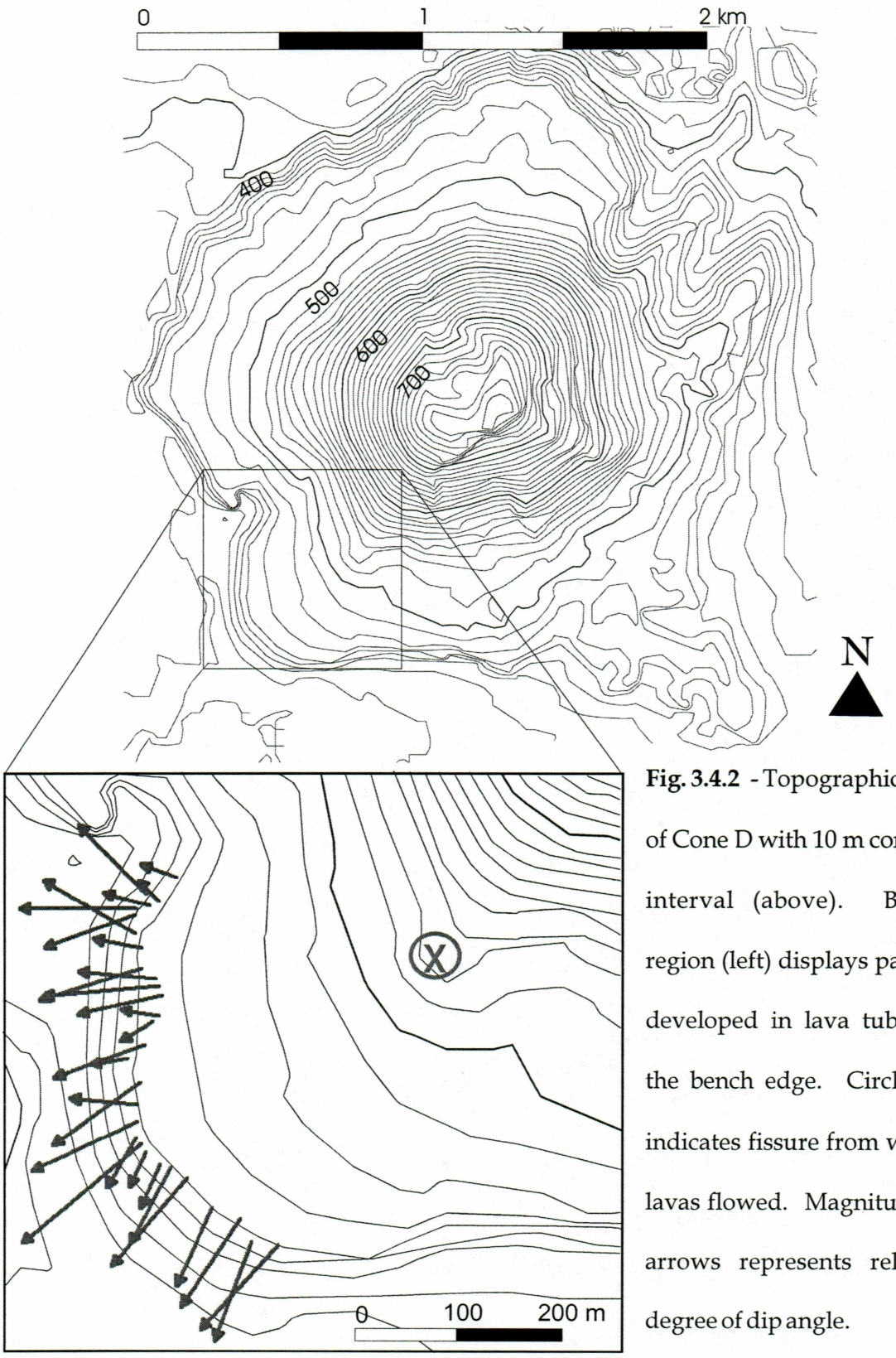

Fig. 3.4.2 - Topographic map of Cone D with 10 m contour interval (above). Boxed region (left) displays pattern developed in lava tubes at the bench edge. Circled X indicates fissure from which lavas flowed. Magnitude of arrows represents relative degree of dip angle.

Table 3.4.1: Lava Morphology Measurements

Tube #	UTM East	UTM North	Direction †	Dip ‡	Dip Error ‡	Min Top Width	Max Top Width	Thick.	Cliff Slope ‡	Tube Width	Tube Thick.	Average Tube Width
T1	692036	5923299	110	4	2	8.0	8.0	3.2	*	*	*	8.0
T2	692017	5923275	135	3	1	6.5	7.0	2.5	*	*	*	6.8
T3	692005	5923282	135	10	2	3.5	3.5	2.5	*	*	*	3.5
T4	692008	5923270	105	5	2	8.0	8.0	3.0	35.0	2.5	*	8.0
T5	691994	5923267	90	12	0	5.0	6.0	6.5	20.0	3.0	*	5.5
T6	691993	5923261	70	10	2	3.5	3.5	2.5	*	*	*	3.5
T7	691993	5923241	120	11	1	6.0	8.0	1.8	20.0	2.5	*	7.0
T8	691999	5923227	100	5	*	11.0	12.0	5.0	20.0	2.5	2.5	11.5
T9	691999	5923205	73	11	*	3.5	3.5	3.0	*	*	*	3.5
T10	692014	5923195	95	8	*	8.0	11.0	3.5	*	*	*	9.5
T11	692017	5923187	85	12	*	3.0	4.0	2.5	*	*	*	3.5
T12	692021	5923178	77	9	*	13.0	15.0	3.0	*	*	*	14.0
T13	692017	5923156	100	4	*	8.0	8.0	3.5	*	*	*	8.0
T14	692011	5923151	57	4	*	4.0	5.0	2.5	38.0	2.5	2.0	4.5
T15	692003	5923127	70	10	*	8.0	15.0	3.5	*	*	*	11.5
T16	691986	5923113	80	4	*	15.0	18.0	4.0	25.0	1.5	1.5	16.5
T17	691986	5923109	60	*	*	10.0	11.0	3.0	*	*	*	10.5
T18	691998	5923088	55	11	*	8.0	10.0	3.0	25.0	1.5	*	9.0
T19	691995	5923066	95	7	*	9.0	10.0	3.5	*	*	*	9.5
T20	691995	5923049	65	12	*	7.0	8.0	2.5	*	*	*	7.5
T21	691994	5923033	30	6	*	6.0	6.0	3.5	25.0	1.5	1.0	6.0
T22	691999	5923026	50	16	*	5.5	6.0	2.5	*	*	*	5.8
T23	692004	5923018	25	4	*	12.0	13.0	2.5	26.0	2.0	2.0	12.5
T24	692018	5923005	23	5	*	7.0	7.0	2.0	*	*	*	7.0
T25	692029	5923002	27	9	*	7.0	7.0	*	20.0	2.0	2.0	7.0
T26	692046	5922991	40	12	*	15.0	16.0	2.5	18.0	1.5	*	15.5
T27	692072	5922961	24	9	*	6.5	6.5	2.0	*	*	*	6.5
T28	692100	5922949	33	11	*	18.0	18.0	3.0	15.0	3.0	2.5	18.0
T29	692112	5922925	20	11	*	7.0	7.0	2.5	*	*	*	7.0
T30	692140	5922922	42	12	*	4.0	4.0	2.0	25.0	2.5	1.5	4.0

Table 3.4.2: Supplementary Measurements

Tube Number	Cliff Slope 2 ‡	Cliff Slope 3 ‡	Cliff Slope 4 ‡	Cliff Slope 5 ‡	Tube Width 2	Tube Width 3	Tube Width 4	Tube Width 5	Tube Thick 2	Tube Thick 3	Tube Thick 4	Tube Thick 5
T8	30.0	22.0	40.0	35.0	1.8	2.5	1.0	1.8	*	2.0	*	1.5
T16	25.0	34.0	*	*	2.5	1.5	*	*	2.4	1.7	*	*
T23	20.0	*	*	*	2.0	*	*	*	1.5	*	*	*
T28	20.0	30.0	*	*	2.5	4.0	*	*	1.5	2.0	*	*

All measurements in meters unless otherwise noted.

† Direction in degrees from north rotating clockwise. Declination of 0° used for these measurements. Actual declination = 11°

‡ Angles in degrees.

* No data collected for this parameter and location.

from a fissure on the south side of Cone D (Fig. 3.4.2). Directly down slope from the fissure, tubes do not extend over the bench edge.

Interpretation – After access of lake water to the vent area had been terminated, degassed lavas were able to erupt effusively and flow out across the volcanic pile from a lava lake. Lavas formed tubes, spread out radially, and then turned abruptly upon reaching the lakeshore, much as was observed during the eruption of Surtsey (Thorarinsson, 1964). This process produced lobate flow terminations and several, partially overlapping, broad fans of lava flows. Flows in the eastern half of Cone D had to circumvent massive tuff beds (Duv) prior to flowing southwest from the vent, and may have degassed or cooled more than their northern counterparts making them more viscous and thicker. We believe our measurements provide a unique data set, as lavas that have erupted historically and then flowed into water at other volcanoes around the world have been reworked by wave action or are submerged and inaccessible to such a survey.

Lava flows comprising Dbl grade into Dcl where they once intersected the paleo-lake after flowing over the bench edge. This transition is a result of lavas chilling in contact with water (Skilling, 2002; D. Lescinsky, pers. comm.). Where no lava tubes or pillows are found downslope from Dbl the flow was fastest, causing lava to explode at the water's edge instead of slipping quietly into the water (c.f., Finch and MacDonald, 1953). Alternatively landslides could have occurred at these locations, removing the tubes and creating steeper slopes (Skilling, 2002).

3.5 Cliff Lavas (Dcl)

Description – Bench lavas that continue over the cliff edge are compositionally identical to Dbl but texturally distinct. Filled lava tubes, with radial fracture patterns in cross section (Fig. 3.5.1), elongate 2-4 cm vesicles, and glassy margins characterize the

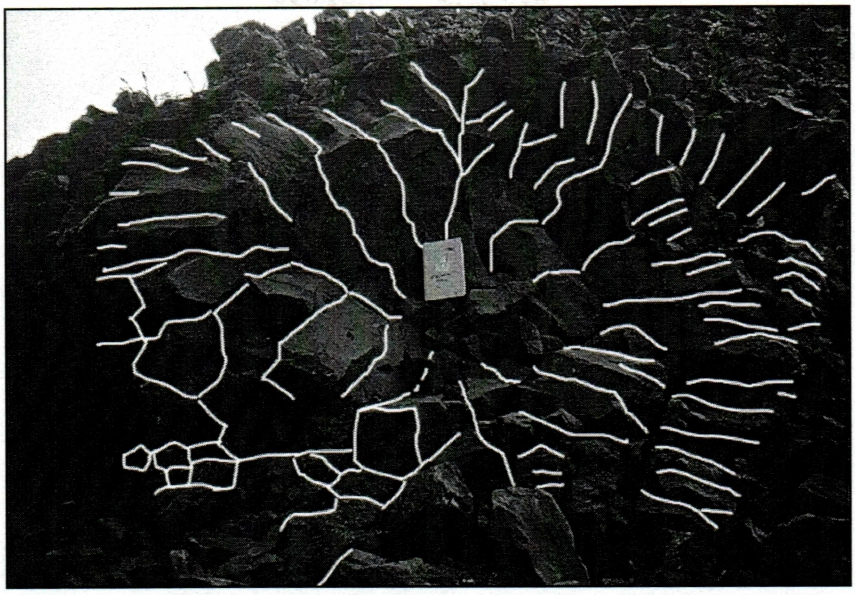

Fig. 3.5.1 Example of radial fracture pattern with decreasing fracture spacing (in white) common to filled lava tubes on Cones C and D. Spacing of fractures is related to cooling speed – closer fractures indicate faster cooling. Field book is 18 cm.

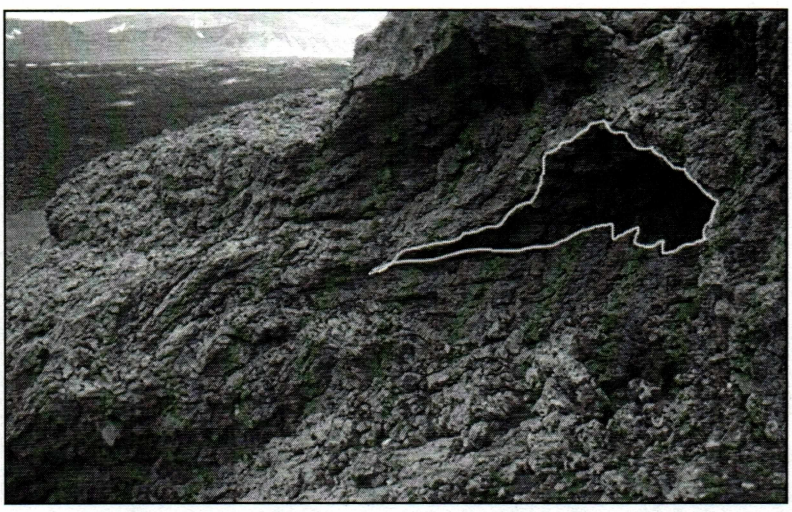

Photo by D.T. Lescinsky, UWO

Fig. 3.5.2 Partially evacuated lava tube on the side of Cone D. Opening, outlined in white, is ~1 m.

uppermost 1-12 m of cliff exposure. Evacuated tubes are found only sporadically along the cliff edge (Fig. 3.5.2). Below this section, fracture patterns become less regular and pseudopillows, hackly fractures, and pillows dominate (Fig. 3.5.3). On steeper cliff edges, tubes are abruptly truncated and end in a pile of fragmented pillows in a palagonitized matrix. Flow toes are found anywhere from directly beneath the tubes to the bottom of the volcanic pile, depending on the pitch of the cliff. Packages of ribbon flows and parallel-sided, anastamosing ridges of basalt with chill margins and polygonal cooling fractures are also found intermittently along the cliff, emanating from the bench lavas above.

At a few exposures, multiple bench lavas flowing out over the cliff edge and then changing dramatically in character are visible. Each successive bench lava flow is visually distinct from the flow below it where not obscured by talus. The elevation at which hackly fracture patterns begin to dominate is higher for each later flow. Pillows, where present, are draped over a hyalotuff interior, directly down slope from lava tubes.

Interpretation – Lavas were able to continue flowing below the water surface through the lava tubes, keeping the interior hot longer and resulting in increased fracture spacing toward the center of each tube. The variation in water-interaction level is contrary to the interpretation of Byers (1959) of a single water level around the bench. The pillows present are also inconsistent with Byers' interpretation of a layer-cake model, with pillows comprising only the lowest layer. Instead, pillows formed downhill from the tubes in places where the cooling rate was higher or the slope angle less than other localities (c.f., Gregg and Fink, 1995). The variety of characteristics found in the cliff flows can be attributed primarily to the effect of effusion rate on degassing and entrapment of water, and degree of slope (Finch and MacDonald, 1953). The lack of evacuated lava tubes is likely due to collapse of these features after emplacement. Some lavas tubes also appear to have flowed farther over the cliff before encountering water,

Fig. 3.5.3 Examples of pseudopillows and hackly fractures from the lower bench of Cone C are highlighted in white. Pseudopillows indicate the entrapment of water or steam within the flow as it cooled, resulting in small, secondary fractures propagating perpendicularly from sets of primary fractures. The chaotic (hackly) fracture patterns with varying orientations and crosscutting relationships result from rapid cooling and explosive interaction with water as it flashed to steam (Lescinsky and Fink, 2000). Field book is 18 cm.

which likely influenced the final morphology. The increasing water interaction elevation for younger flows indicates that the lake level was rising as the edifice was building up.

Debris from pillow-fragment breccias likely formed bedded deposits with the slope influenced by the component of coherent lava within the breccia. Slopes below water level would be less stable than their subaerial counterparts, resulting in frequent slumping and debris flows. As each subsequent lava flow reached the bench edge, it would be subjected to higher strain rates as it suddenly flowed over steeper terrain, making it more likely to be fragmented. Thus the steepening process around the bench edge would have a positive feedback.

3.6 Cinder Cone (Dcc)

Description – A 260 m cone composed of vitreous and oxidized 3-5 cm scoria, cinders, and spatter agglutinate at the angle of repose sits in the center of Cone D's lava bench (Fig. 3.6). The crater is a broad (~250 m) shallow (~30-40 m from rim to base) bowl opening to the NE. Crusts of white, yellow, and red salts and clays rim parts of the crater, but we observed no active fumarolic activity.

Interpretation – A strombolian eruptive phase ensued once water no longer had access to the vent region. We assume that the cinder cone is coeval with Dbl and Dcl, the style of eruption being dependent upon the magmatic volatile content during each eruptive phase. Eruptions likely progressed from strombolian to hawaiian-style as each magma batch degassed (Wilson, 1980). Modern observations at Cone A support the hypothesis of concurrent cinder pile and lava flow growth as both effusive and explosive activity have been noted during the same eruption from a single vent. It is possible that the strombolian phase of eruptive activity continued subsequent to all other eruption types to build Cone D to its current height.

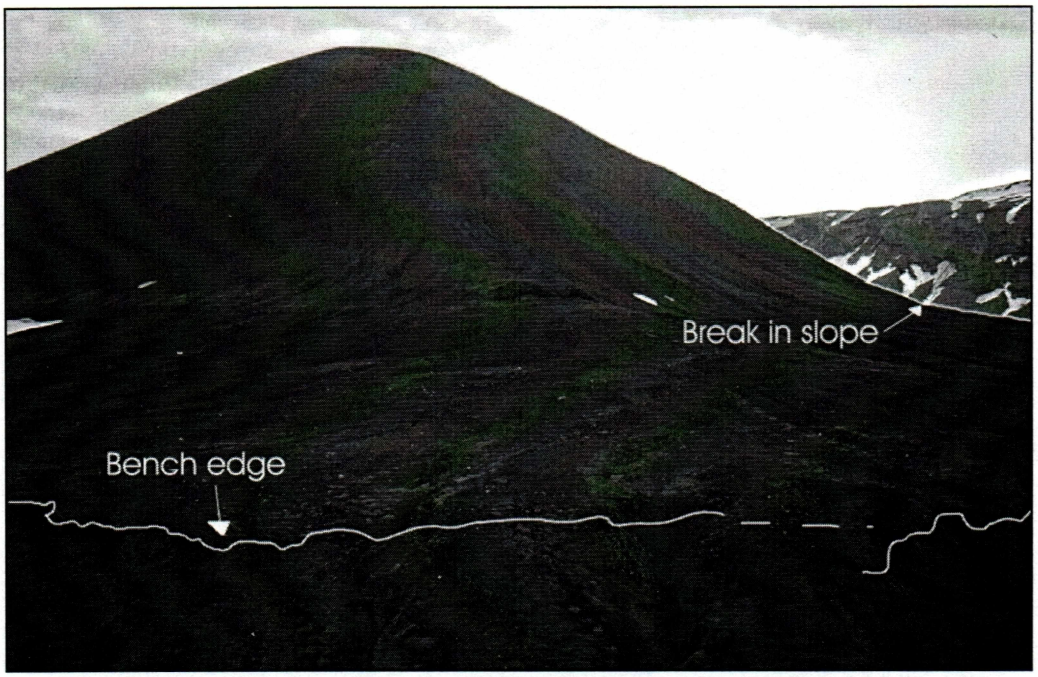

Fig. 3.6 The cinder pile of Cone D rises 260 m above the surrounding lava bench. The break in slope indicates the highest elevation attained by the lake. The bench edge developed as lavas encountered the lake at a lower elevation earlier in the cone's evolution.

3.7 Lacustrine Deposits (Dl)

Description – Yellow, orange and brown laminated silt and clay layers (5-20 cm) intercalated with coarse, angular, clast-supported, gravely layers and coarse sands mantle the upper bench surface. Contortions of lamane and flame structures are visible in some clay layers. Forset beds of coarsening upward scoria (5 cm), separated by local ash beds 3-6 cm thick, overlie clays, sands and gravels.

Interpretation – Periods of quiescent deposition in a lacustrine environment are necessary for the development of finely laminated silt and clay beds. These quiet periods are punctuated by deposition of reworked cinders from Cone D and eruptive products from elsewhere in the caldera. Cone D shows no signs of eruptive activity after the lake level was high enough to cover its bench. We believe the laminae contortions and flame structures are due to plastic deformation of lacustrine deposits caused by seismic activity within the caldera.

3.8 Surge Deposits (Ds)

Description – A massive, dark gray, fine-grained, unconsolidated unit (>2 m) mantles the bench deposits and marks a sharp slope break around the cinder cone. Abundant accretionary lapilli, 4-5 mm in diameter, are present throughout. These deposits and the underlying Dl unit are absent from the lower half of the bench surface, with sediment thickness decreasing rapidly away from the center of Cone D. The present extent of Ds and Dl is radial and finger like in plan view (Appendix A).

Interpretation – Prior to the catastrophic breaching of the caldera wall by the lake, surges were formed by the eruption from another intra-caldera cone through the caldera lake. Deposits from this eruption thickly mantled the upper bench surface of Cone D where the water was the most shallow. The final catastrophic flooding event ensued shortly

thereafter, stripping the loose sediments off the lower flanks of Cone D's bench and redistributing sediments throughout the caldera.

CHAPTER 4: WATER STORAGE IN OKMOK CALDERA

4.1 Caldera Lakes

In their preliminary investigation of Okmok Caldera, Byers and others (1947) and Byers (1959) found extensive evidence for a caldera-filling lake, including laminated fine sediments inter-bedded with gravels, pillow basalts, and wave-cut scars on Cone D. Their observations indicated that there had been two lake filling and subsequent flooding events, which emptied the crater of water. Previous workers at Okmok have made estimates of the total volume of water contained within the paleo-caldera lake. Wolfe's (2001) estimate of 5.8×10^9 m^3 was based on a simple cylindrical lake shape using an average lake depth of 150 m and a maximum lake extent of 39 km^2.

Using the volume calculation method described in Chapter 2, I have determined a more accurate lake volume estimate of 4.3×10^9 m^3. This takes into account the volume of lake water displacement due to the sublacustrine volcanic cones and lava flows that had begun refilling the caldera and uses an irregular, not circular, shoreline defined by the equipotential lake surface within the caldera.

Wolfe and Begét (2003) describe in detail large-scale geomorphic features they use as evidence for a catastrophic lake-draining event between 1560 and 1010 radiocarbon yr. B.P. The breach in the caldera wall, where the current Crater Creek drains the existing caldera lake, contains coarse boulder deposits more than 40 m above the gorge floor. Additional flood-type deposits fan out of the caldera from the gorge, including elongate trains of large (>1 m) boulders, abandoned stream channels, streamlined erosional landforms, and a large fan of boulders extending several kilometers into the Bering Sea beyond the limits of the former shoreline.

Evidence for the depth of the smaller, younger caldera lake is sparse. It appears to have drained in relation to an eruption within the caldera in 1817 c.e. (Wolfe and Begét, 2002). Deposits from the smaller flood mantle the earlier flood deposits on the

flanks of Okmok. Within the caldera, however, evidence for refilling of the lake has been obscured by lava flows from Cone A and the present lake which was dammed by the 1958 flow to the north of Cone D. Byers' (1959) map of the lake deposits on the caldera floor and a photograph of the wave-cut scars on the side of Cone D's bench (Byers et. al 1947) provide additional evidence of the existence of a second crater lake.

4.2 Glaciology

On 16 August 2002, I carried out an investigation near the terminus of what had been mapped (Byers 1959) as a glacier hugging the southern rim of the caldera wall. Previous workers in the caldera (Byers 1959; Burgisser, pers. comm.) have suggested that the glacier was "dead," having been mantled by tephra and undermined by flows from Cone A, which it abuts. Heretofore no glaciological measurements of the ice body have been attempted, thus I excavated a snow pit in an effort to glean some information about the health of the glacier and its annual accumulation.

It was not possible to excavate a pit deeper than about 1 m by hand due to an impenetrable layer of frozen tephra (possibly from the 1997 eruption). Twelve cm of firn (multi-year snow) underlies a 5 cm superimposed ice lens, above the frozen tephra. The top 70 cm consisted of homogeneous first year snow. Since these measurements were made at approximately the end of the ablation season, I can say that there was net accumulation of 75 cm on the glacier in 2002 (noted unofficially by locals to be a "low-snow year").

Burgschrunds (deep, transverse crevasses) ringing the headwall of the glacier indicate flow processes are still active in the upper part of the glacier (Benn and Evans, 1998). The terminus of the glacier is steep (~18°), indicating that the glacier is growing (Post and LaChapelle, 2000). This is logical due to the two volcanically influenced factors that create a positive net balance for the ice body: 1) the ablation zone has been

truncated by growth of Cone A, leaving almost the whole glacier within the inferred accumulation zone; and 2) thick tephra deposits from the 1958 and 1997 eruptions mantling the glacier insulate the ice and prevent ablation from its surface.

CHAPTER 5: HYDROVOLCANISM

To understand the volcanic processes acting in an environment as described previously, I turn first to experimental work that has been done and then to the records of historic hydrovolcanic eruptions and geologic evidence for similar events in the past.

5.1 Water Magma Interactions

The primary controls on eruptive style in a hydrovolcanic setting, determined by experimental results (Wohletz, 1986) and field observations (Houghton and Smith, 1993), are the proportion of magma to water (i.e. fuel/coolant ratios). Other factors are original volatile content, temperature, viscosity, and volume of the magma, plus the water temperature, pressure, and salinity. Wave action also plays a role in allowing water to access the vent and in reshaping and distributing volcaniclastics in a marine environment. When magmas interact with ground water, wall rock coherency, geometry and total overburden provide additional complexities controlling the eruptive style.

In cases where the hydrostatic pressure is great and/or the original volatile content of the magma is low (>0.5%), eruptions tend to be effusive and comminution of lavas is strictly due to spallation of cooled pillow surfaces, leading to the formation of hyaloclastites (Kokelaar, 1986). By either decreasing the water depth above the vent or increasing the dissolved volatiles within the magma, eruptions become more violent, explosions more common, and comminution of lavas more complete. Honnorez and Kirst (1975) define pyroclastic rocks generated in such a manner as 'hyalotuffs'.

The effusion rate is also important in determining how vigorously magma and water will interact. Hawaiian lavas have been observed to slip quietly into the ocean when effusion rates were low, and to cause great explosions forming littoral cones when entering the water faster and in larger volumes (Finch and MacDonald, 1953). This may

be a result of faster lavas entrapping more water, which then explodes as it flashes to steam, or that they are less degassed and therefore more likely to explode.

Researchers have calculated a wide range of values for the volatile fragmentation depth, the depth at which eruptive activity begins to transition from effusive to fragmental. Kokelaar (1986) determined minimum depths of 100-200 m for basalts to begin fragmentation upon eruption, even with low (0.1%) volatile contents. Basalts are unlikely to erupt effusively at shallower water levels unless completely degassed.

When the ratio of melt to water reaches a critical value (0.31, Wohletz, 1986), eruptions become extremely violent. This optimal degree of mixing is often met at the site of emergent volcanoes. Base surges, explosions large enough to alter the vent location, tephra jets, and shock waves in water are all results of the thermodynamic processes acting upon contact of water and magma. Most of the energy released is consumed in fragmenting, not in dispersing, pyroclastics. Fall deposits from tephra jets commonly extend only a few hundred meters to a few kilometers from the vent (White and Houghton, 2000), in contrast to plinian fall deposits that can cover 10-100 times that distance.

Eruptive activity from emergent vents typically evolves from surtseyan to strombolian, to lava fountaining and/or effusive eruptions as water looses access to the vent region and magma is degassed (White and Houghton, 2000). Thus, if an eruption is sustained long enough for the vent to dry out, it is possible for a subaerial pile to be built upon subaqueously erupted material. Wave erosion is effective in removing subaerial volcaniclastics unless they are armored by lava flows, as was observed during the formation of Surtsey (Thorarinsson, 1964) and appears to have happened over sections of Cones C and D in Okmok Caldera.

5.2 Historical Emergent Eruptions

Geologists have had the opportunity to actively monitor only a handful of emergent eruptions. All other knowledge of the processes that take place as a volcano breaches the surface of a lake or the sea is based on remnant features within drained lakes and samples recovered on deep-sea dives or from drill cores. Observations of Surtsey's formation, off the southern coast of Iceland, were particularly important in understanding hydrovolcanism.

5.2.1 Lessons from Surtsey

Surtsey's emergence began early in November of 1963 with the stench of sulfur in the air, an increase in water temperature around the vent region, and a darkening of the water above the vent (Thorarinsson, 1964). Thorarinsson and others closely observed the ensuing eruptive events over the following year from ship decks, aircraft, and quick forays onto the island itself. Their observations brought new insights into the processes active during an emergent volcanic event.

Geologists made three key observations during the event at Surtsey that are relevant in explaining features forming Cone D: different eruptive styles when water had direct access to the vent and during dry eruptions; the build-up of an asymmetric tephra pile caused by a prevailing wind direction during eruptions; and sharp changes in direction of lava rivulets upon contacting sea water.

Thorarinsson (1964) noted that while the sea had access to the vent, either directly or through the scoria walls, the activity was similar to what had been seen in other submarine eruptions. He and others saw tephra rich plumes blasted out of the vent after each explosion, and turn from black to grayish-white as superheated vapor cooled in the air. The trajectory of the plumes was dependent on the depth within the vent where the explosion happened. Deeper explosions sent tephra columns vertically

as much as 500 m and occasionally lobbed lava bombs up to 1000 m, whereas explosions higher in the vent formed curved, cock's tail tephra jets (Fig. 5.2).

When water could not access the vent, tephra and vapor rushed continuously upward, sending up columns 1-2 km in height. Observers noted that far more tephra was produced during such continuous eruptions than during the intermittent explosive activity.

Thorarinsson (1964, pp 42) briefly mentions the effect of winds on tephra dispersion; "while the northerly wind lasted the southern end of the fissure often got blocked by a tephra wall, giving the island the shape of a prolonged horseshoe with an opening towards northeast." It is conceivable that such a process built the underlying benches of Cones C and D, since strong winds are forced across the caldera away from the wall at these localities.

The marked change in course of lava flows described by Thorarinsson, and displayed in photographs taken during the effusive stage of Surtsey's development, matches the fanning-out pattern of flows measured on Cone D (see Fig. 3.4.2 and Appendix B). The directional change of lava rivulets is due to more rapid cooling of lavas in contact with water than of those in air. Lava flows at Surtsey protected the tephra cliffs from further erosion by the sea and similarly preserved, at least in part, the original tephra piles of Cones C and D.

5.2.2 Other analogous emergent eruptions

It is instructive to look at other examples of historic emergent eruptions to fully understand the mechanisms that were likely requisite for the formation of Cone D. I incorporate such observations to help explain features of Cone D, and to a lesser extent Cone C. The eruption of Capelinhos Volcano, Island of Faial, Azores bears a great resemblance to both the setting and the probable sequence of events within Okmok

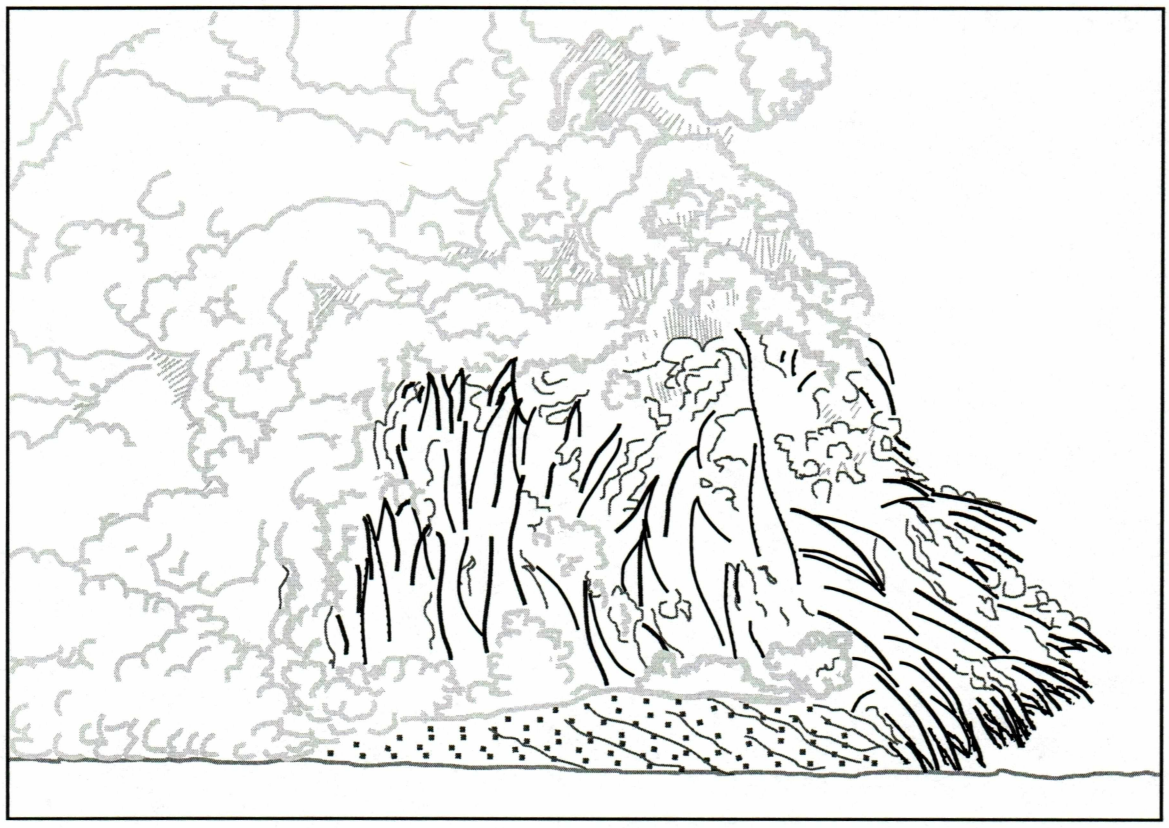

Fig. 5.2 Sketch of cock's tail tephra jets and accompanying steam plume formed as Surtsey breached the sea surface off the south coast of Iceland (After Thorarinsson, 1964, plate 10).

Caldera as Cone D was built. The Island of Faial is a large shield volcano with a central caldera, surrounded by the Atlantic Ocean and dotted with numerous satellite cinder cones and maar volcanoes.

Hydrovolcanic activity began in 1957 (Waters and Fisher, 1971) with the formation of a complex maar volcano. A small tuff ring was subsequently built above the sea surface and quickly destroyed by wave action. The present tuff cone was built up more than 150 m above sea level. Water was excluded from the vent during the final stages of eruptive activity, changing the eruptive style from phreatomagmatic to lava fountaining and effusive activity. Lava flows built seaward from several subaerial vents and protected the friable unconsolidated tuffacious deposits from wave erosion.

5.3 Subaqueous and Emergent Eruptions in the Geologic Record

Godchaux and others (1992) detail the lithofacies variations of emergent, subaqueous and subaerial cones in the Snake River Plain of Idaho. Their lithofacies descriptions are similar to the deposits found within Okmok Caldera. They subdivide the deposits from emergent cones into three sub-sets: basal massive deposits, bedded tuffs, and late magmatic deposits. Of these, the second is most similar to the exposures of Duh found on Cone D. They report thin planar beds of oxidized non-palagonitized and partially palagonitized lapilli tuff lying unconformably over the basal massive deposits. They also find bomb and block sags within these deposits and secondary minerals, such as calcite in the lower beds. These beds are reported to be overlain by thicker-bedded, finer-grained mostly palagonitized tuffs with well-developed, undulatory surge cross bedding. Capping most of these emergent volcanoes are welded-spatter deposits and local dike-fed lava flows.

Christensen and Gilbert (1964) give a brief description of a flat-topped, conical accumulation of sub-horizontally stratified basaltic cinders and tuff-breccia, built within

Pleistocene Lake Russell (now Mono Lake), California. A more detailed investigation of this feature (Custer, 1968) reveals much about the structure and eruptive environment of Black Point. The edifice, with a total volume of 0.83 km^3 and a height to width ratio of roughly 1:24 (compared to 0.59 km^3 and 1:20 for Cone D), now rises completely above the current lake level. The vent region is estimated to have been under approximately 100 m of water at the onset of volcanic activity. Custer's evidence indicates that the eruption terminated shortly after breaching the paleo-lake level.

Custer (1968) found Black Point to be comprised of two primary lithofacies, generally layered and horizontal, but with complex relationships in detail. A base of unconsolidated, unaltered tephra underlies a consolidated, well-indurated tephra (tuff). The upper part of the tuff has been palagonitized. The neighboring islands of Paoha and Negit (also within Mono Lake) are reported to have volcanic cinder cones and lava flows that are hypothesized to overlie deposits similar or identical to those of Black Point.

White (2001) gives a detailed description of the lithofacies variations within Pahvant Butte, Utah. He developed a model for how these lithofacies were developed in the shallow (85 m) waters of Pleistocene Lake Bonneville, based on volcanic and sedimentary processes. He describes a basal unit of fines-poor, well bedded, broadly scoured beds of sideromelane tephra with localized low-angle cross-stratification. These are observed to grade upward into a lithofacies characterized by progressively better-developed dunes and cross-stratification. The first two units are inferred to have developed below the syneruptive lake level and have been emplaced mostly by traction from dilute sediment gravity flows generated during eruption. Two other lithofacies are found intercalated with the two lower units. They are described as weakly bedded tuff and breccia, and nearly structureless units with coarse basal layers above strongly erosional contacts.

The morphology illuminated by multibeam echo sounding within Crater Lake, Oregon (Bacon et. al., 2002) is broadly similar to that of Cones C and D. Wizard Island is composed of sequences of lava deltas (inferred to record former lake levels) beneath a central cinder cone. The bench edges have more gentle slopes and are up to two times higher than those measured in Okmok Caldera, but this may be due to differences in composition (andesite versus basaltic andesite), time since emplacement for mass wasting to occur (c.a. 7700 yr. B.P. versus c.a. 2050 yr. B.P.), or estimated effusion rate (2.6 km^3 over c.a. 400-750 yr versus 0.59 km^3 in approximately the same amount of time).

Skilling's (2002) detailed description of lava delta facies in Antarctica and compilation of similar such studies from other workers clearly illustrates the process of lava delta formation. He describes the concave upward, wedge-shaped packages of lava breccias that reveal how lava deltas build up and out to form steep sided benches above shallowly dipping beds of hydrovolcaniclastic materials. Coarse, blocky material is deposited directly down slope from where lavas enter water, leaving smaller amounts of finer material to be deposited down slope, resulting in oversteepened delta benches.

CHAPTER 6: DISCUSSION OF ERUPTIVE SEQUENCE

The descriptions of lithological units, accounts of historic hydrovolcanic eruptions, and observations of emergent volcanism in the geologic record can be assimilated into a cohesive package that explains the sequence of events that transpired to form Cone D in Okmok Caldera. I generalize from this sequence to explain features observed throughout the caldera by other workers.

Immediately following caldera collapse the crater behaved as a giant catchment basin for the ample meteoric and ground water characteristic of the Aleutian Islands, and a lake began to form in the caldera. Activity in the vicinity of the proto-Cone D was initiated into relatively shallow water (<100 m), based on the lowest evidence for emergence, thus forming either maars or low profile tuff rings as the magma exploded violently upon contacting ground and lake water (Wohletz and Sheridan, 1983). These deposits cannot be sampled directly, but this is the most likely scenario based on deposits in similar geologic settings (Lorenz, 1986) and observations from historic eruptions in similar environments (Self, 1980). Following the argument that the lake level was rising over the duration of activity from Cone D's vent, it is unlikely that the basal unit is constructed of pillows. The earliest stages of the eruption would likely have been volatile-rich and therefore explosive, since the shallow water would not have been sufficient to suppress gas expansion of the magma.

The lowest stratigraphic unit I find on Cone D, Dlh, initially erupted into water 60-80 m deep. As the tuff ring grew, vertically and laterally, the massive facies represented by Dlh built up by gravity flow and tephra jet fallout to or above the lake surface (Fig. 6.1 A). What remains of this tuff cone is only the remnant of a distal tuff arm forming a small peninsula extending out into the present crater lake.

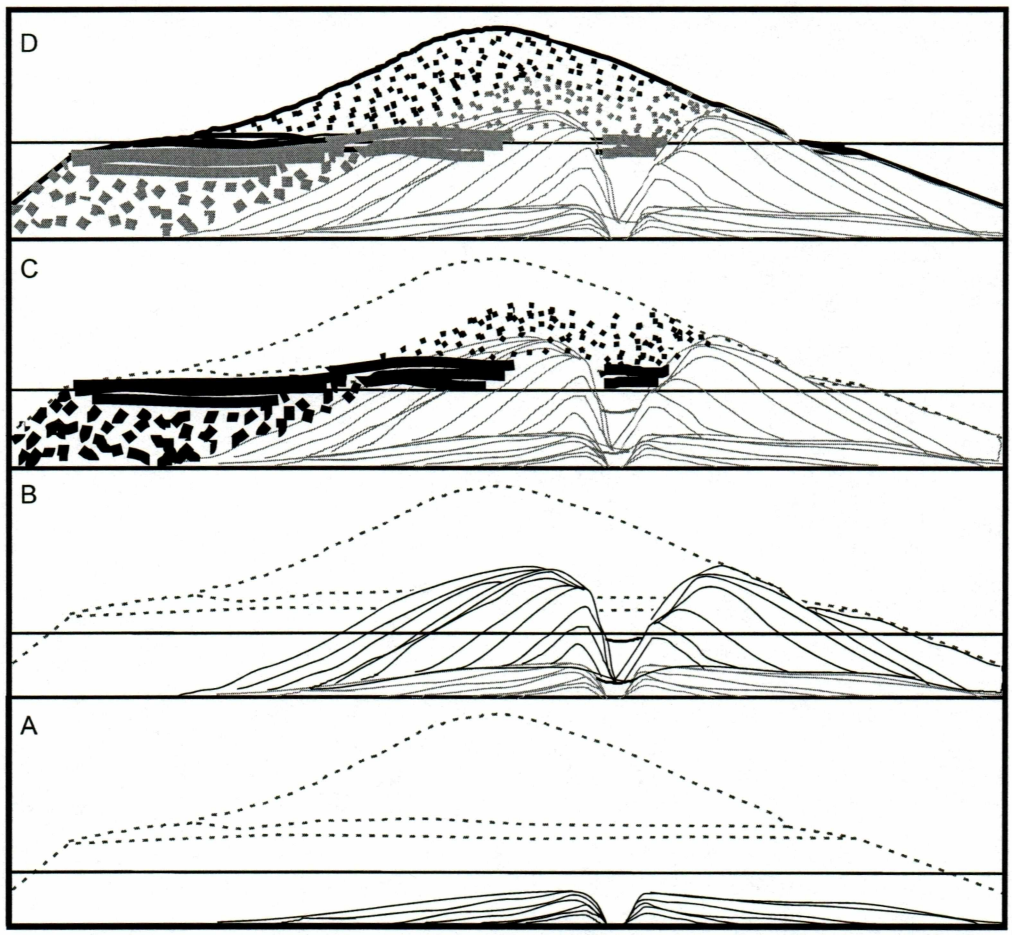

Fig. 6.1 Generalized eruptive sequence of Cone D's construction. Total cone height is ~400 m . Horizontal line across each scene indicates the inferred water level. A) tuff ring develops in shallow water (<100 m). Gravity flow is primary transportation mechanism; B) as the vent elevation increases, the attitude of the tuff beds changes and a tuff cone begins to build, with its crater rim above the lake level; C) the lake level continues to rise, but the vent is now shielded from water by the tuff cone. Pahoehoe flows spread laterally over the tuff pile from a lava lake then turn abruptly upon reaching the lake. Lavas brecciate and form steep slopes below the lake surface; D) strombolian activity becomes dominant and builds the cinder cone to its current elevation. The lake rises to its maximum elevation of ~510 m a.s.l. Lacustrine and surge deposits mantle the lava deltas.

Following the emplacement of this tuff ring, there appears to have been a hiatus in the eruptive activity or a change in vent geometry with relation to relative water depth, demarcated by the unconformable contact between Dlh and Duh. The repose period between the two eruptive events was long enough for the beds of Dlh to be roughly planed off at 391 m ASL as the water rose, but not long enough for them to cool below 100°C. The rootless fumaroles that cut through the beds of Duh indicate incipient boiling of lake water and support the argument for hot, shallow beds.

The first vent I can approximately locate lies about 250 m east of the final, strombolian phase vent. This vent appears to have been active throughout a long and cyclical eruptive phase, building up more than 100 m of bedded tuff deposits about its crater rim to well above the lake surface (Fig. 6.1 B). The radial arms of Duv were likely formed during this interval of tuff cone formation, eventually building an edifice similar in morphology and size to Cone G on the western arc of the caldera floor. The final eruptive stage for this vent was relatively dry, and much vent wall material was recycled, as evidenced by the large blocks of indurated material in the upper-most beds of this unit.

A shift of the eruptive center to the west produced a new vent armored on its eastern flank by the massive tuff cone, preventing water from rushing in on that side and lava flows from spreading in that direction. As the vent dried out completely, the eruptive behavior shifted from the previously surtseyan dominant style to strombolian or hawaiian, depending on the degree of degassing prior to eruption. It is conceivable that each eruptive phase, after the vent dried out, began with a rush of strombolian activity, throwing cinders high into the air, building up the massive cone, and filling in previous craters, followed by more quiescent hawaiian activity as pahoehoe flows oozed out of flank vents (Fig. 6.1 C).

The degassed pahoehoe flows turned abruptly as they encountered the rising lake water, fanning out and forming the large lava deltas clearly distinguishable today around the north to southwest circumference of Cone D. The outsides of the slowly flowing lavas cooled quickly, forming tubes that allowed lava to continue to flow under water before breaking off into small pillow fragments. The rapidly cooling lavas were fractured in a wide array of patterns controlled by interactions with the surrounding water and steam. Empty lava tubes collapsed and pillow fragments accumulated to form a lava breccia under water, creating a bench for subsequent lava flows to extend out further over.

As activity at Cone D's vent began to taper off and the lake continued to rise, lacustrine sediments settled out of the turbid water filled with tephra deposits from other still active cones within the caldera. Occasionally these finely laminated beds were disturbed by the frequent seismicity within Okmok, contorting the plastic layers. Scoria lapilli from Cone D continued to rain down intermittently forming coarser deposits between the layers of silt and sand (Fig. 6.1 D). Wave action within the lake would have gradually reworked unconsolidated tuffacious material, planing off tuff arms near lake level, ~500 m ASL.

Phreatomagmatic eruptions from other cones within the caldera formed basal surges, which are recorded in the youngest deposits on Cone D. No other water-laid deposits cap these surge deposits, indicating that the lake began to drain at or near the time of one of the surge-forming eruptions from an unknown source. These deposits, along with the underlying lacustrine sediments are mostly absent from the lower half of the bench. What remains of these deposits reaches its maximum thickness around the base of the cinder cone, decreases down slope in radial finger-like projections and disappears completely less than 100 m from the bench edge. The remnant distribution of the lacustrine and surge deposits appears to have been shaped by the catastrophic

draining of the lake, as all ridges of sediments around Cone D point roughly in the direction water would have rushed toward the breach in the caldera wall.

CHAPTER 7: EFFUSION RATES

The unique set of circumstances within Okmok Caldera, combined with the high-resolution DEM for the island, allowed me to calculate approximate effusion rates for the first half of the caldera's existence. I compared the calculated paleo-effusion rates with historical effusion rates to increase understanding about magma production in this highly active Holocene volcanic center over the past 2000 years.

A simple relationship of volume erupted, during a dated time interval for which marker beds are found, over the selected time period was used to calculate effusion rates. Volumes for pre-historic eruptions were calculated using the DEM and the volume calculation program in PCI Geomatica™ as described previously. Elevations from which to calculate volumes were based on field relationships of lithofacies determined during the 2002 field season.

Several sources of data were used to calculate the volumes of eruptions from Cone A: for all deposits older than the 1958 lava flow, the area of each flow, as mapped by Byers (1959), was determined using Scion Image. I then multiplied the area by the average thickness as reported by recent workers within the caldera (K. Papp and D. Grey, pers. comm.). The area and thickness of the 1958 lava flow were measured using aerial photographs and field measurements (D. Grey, pers. comm.). The volume of the 1997 flow was taken from recent work by K. Papp and M. Patrick (pers. comm.) using remote sensing techniques to find the difference in ground elevation, over the flow area, prior to and after the eruption, equal to the total flow volume.

7.1 Cone D

I believe the entire volume of Cone D erupted between the collapse of the caldera at 2050 yr. B.P. and the first catastrophic flood between 1560 and 1010 yr. B.P., based on

the field evidence cited previously. The radiocarbon calendar dates from Wolfe (2001) allow a window of opportunity between 435 and 1114 years for the edifice to grow. Because the bracketing radiocarbon dates are based on organic soils found above and below flood deposits, I can assume that the event is younger than the oldest possible age, since the flood event would likely have eroded the substrate prior to deposition. For lack of better constraining dates at the time of writing, I choose a date half way between the maximum and minimum for the flooding event as the time of incidence. Thus the lake is presumed to have occupied the caldera for c.a. 775 years.

The total volume of lacustrine and surge deposits mantling the lava bench is negligible compared with the volume of the rest of the cone, and is likely small compared to the pyroclastic products which would have been dispersed beyond the study area during energetic eruptions, therefore I incorporate them in the calculation of the total volume of products erupted from this vent, although they likely did not originate from it.

The total volume of Cone D is 0.59 km^3. This includes the cinder cone and the lava bench down to the approximated caldera floor at this location (350 m ASL), based on the lowest caldera floor elevation. Dividing the volume by 775 years gives an approximate effusion rate of 0.8×10^6 m^3yr^{-1} for this vent. The possible range of effusion rates for this vent, based on the available radiocarbon dates, is from 0.5×10^6 m^3yr^{-1} to 1.4×10^6 m^3yr^{-1}.

7.2 Total Effusion During Lake Period

The lithofacies and morphologies of Cones C, K, and G, although not described in this work, all show extensive evidence of having interacted with a significant amount of water (USGS/AVO unpubl. map). Based on this interpretation, I assume that the bulk of the pyroclasts for each of these cones was extruded prior to the lake draining

event. Therefore I have calculated the total volume for these cones to derive the effusion rate for the first 775 years after caldera collapse. The total volume of the five subaqueous or emergent cones is 2.1 km^3, giving a post-caldera forming effusion rate of 2.7 x 10^6 m^3yr^{-1}. This is an underestimation as it does not take into consideration surge and deposits on the volcano flanks or flood rafted material.

7.3 Recent Effusion

Cone A appears to have been the primary cite of eruptive activity in Okmok Caldera during the past century. Two massive lava flows from Cone A spread out across more than 9 km of the caldera floor after the first geologic mapping initiative on the island in the 1940s, just after emplacement of the relatively small 1945 lava flow. Cone A itself is a massive 4.3 x 10^8 m^3 pile of cinders and ash, built up from repeated strombolian events.

The total volume of products erupted from Cone A increased substantially with each subsequent event since the vent became active. The approximate total volume of several flows measured collectively as "pre-'45 flows" is 0.68 x 10^8 m^3, the 1945 flow is 0.36 x 10^8 m^3, the 1958 flow is approximately 1.21 x 10^8 m^3, and the 1997 flow is 1.36 x 10^8 m^3. The volumes of these flows taken together with the cone itself over the past c.a. 150 years gives an effusion rate of 5.27 x 10^6 m^3yr^{-1}. This is comparable to the shallow magma chamber refilling rate predicted from SAR interferometry modeling (Mann et. al., 2002).

Table 7.3 Volumes and Calculated Effusion Rates

Deposit	Eruption Period (yr. BP)	Volume ($x10^8$ m^3)	Time Averaged Effusion Rate ($x\ 10^6$ m^3yr^{-1})
Cone D	2050 > t > 1010	5.9	0.8
Cone C	2050 > t > 1010	5.7	0.7
Tuff Cones	2050 > t > 1010	9.4	1.2
Total pre-flood products	2050 > t > 1010	21	2.7
Cone A	200 > t > present	4.3	2.9
Pre-'45 A flows	200 > t > 58	0.68	0.7
1945 A flow	58 > t > 45	0.36	2.7
1958 A flow	45 > t > 6	1.21	3.1
1997 A flow	6 > t > present	1.36	---
Total A products	200 > t > present	7.91	~5.3

CHAPTER 8: CONCLUSIONS

After the 2050 yr. B.P. caldera-forming eruption, Okmok Caldera began filling with water. New volcanic vents began to erupt into this nascent lake and the products erupted were shaped by the interaction of magma and water. A unique opportunity for study was created when the crater wall was breached and the lake drained, exposing a wide range of hydrovolcanic deposits that formed only 1000-2000 years ago.

Our survey of Cone D revealed that it was formed by a series of eruptions as the caldera lake deepened. The first facies that developed Dlh, Duh, and Duv record the interaction of magma and water as the edifice built up to and eventually breached the lake surface. After water no longer had access to the vent lava flows (Dbl and Dcl) were able to form out over the sublacustrine tuff pile and a cinder cone built up above the lake surface. I found substantial evidence to support a maximum age of Cone D that is older than the first catastrophic flood, including the lacustrine sediments (Dl) and surge deposits (Ds) mantling the lava bench. With these bounding ages for development of this cone and an accurate volume calculation based on DEM data, I calculated an effusion rate of 0.8×10^6 m^3yr^{-1} for this vent. This estimate is accurate ± 30%, based on the range of possible ages for the flooding event.

I then calculated an average paleo-effusion rate of 2.3×10^6 m^3yr^{-1} for the entire volcanic system by correlating our observations on Cone D with unit descriptions made by other workers throughout the caldera. I compared this estimate with the calculated historic effusion rate from the active Cone A.

These calculations showed that the effusion rate for these two discrete time periods is within the same order of magnitude. Without better constraints on the timing of the first catastrophic flood and the volume of surge deposits outside of the caldera it is difficult to further refine my calculations. The larger picture of magma production within Okmok Caldera could be more fully understood by constraining the above

parameters and carrying out a similar investigation for the volcanic features developed between the two time periods explored here.

REFERENCES

Bacon CR, Gardner JV, Mayer LA, Buktenica MW, Dartnell P, Ramsey DW, Robinson JE (2002) Morphology, volcanism, and mass wasting in Crater Lake, Oregon. GSA Bulletin 114(6): 675-692

Benn DI, Evans DJA (1989) Glaciers and glaciation. Oxford University Press, Inc., New York, pp 734

Byers FM (1959) Geology of Umnak and Bogoslof Islands, Aleutian Islands, Alaska. In Casadevall TJ (ed) Investigations of Alaskan Volcanoes U.S. Geological Survey Bulletin B 1028-L, pp 267-369

Byers FM, Fisher B, Bernard Hopkins DM (1947) Volcano investigations on Umnak Island: U.S. Geological Survey Alaskan Volcano Investigations Report 0002. pp 19-53

Cas RAF, Landis CA, Fordyce RE (1989) A monogenic, Surtla-type, Surtseyan volcano from the Eocene Waiakera-Deborah volcanics, Otago, New Zealand: a model. Bull Volcanol 51: 281-298

Christensen MN, Gilbert CM (1964) Basaltic cone suggests constructional origin of some guyots. Science 143: 240-24

Custer SG (1968) Stratigraphy and sedimentation of Black Point Volcano, Mono Basin, California. Unpubl MSc thesis, University of California, Berkley, pp 110

Finch RH, MacDonald GA (1953) Hawaiian volcanoes during 1950. Report to the Hawaiian Volcano Observatory. U.S. Geological Survey Bulletin, 996-B, pp 27-89

Godchaux MM, Bonnichsen B, Jenks MD (1992) Types of phreatomagmatic volcanoes in the western Snake River Plain, Idaho, USA. J Volcanol and Geotherm Res 52: 1-25

Gregg TKP, Fink JH (1995) Quantification of submarine lava-flow morphology through analog experiments. Geology 23(1) 73-76

Hickson CJ (2000) Physical controls and resulting morphological forms of Quaternary ice-contact volcanoes in Western Canada. Geomorph. 32: 239-261

Honnorez J, Kirst P (1975) Submarine basaltic volcanism: Morphometric parameters for discriminating hyaloclastites from hyalotuffs. Bull Volcanol 39(3): 441-465

Houghton BF, Smith RT (1993) Recycling of magmatic clasts during explosive eruptions: Estimating the true juvenile content of phreatomagmatic volcanic deposits. Bull Volcanol 55: 414-420

Jakobsson SP, Moore JG (1986) Hydrothermal minerals and alteration rates at Surtsey volcano, Iceland. Geological Soc Am Bull 97: 648-659

Kokelaar P (1986) Magma-water interactions in subaqueous and emergent basaltic volcanism. Bull Volcanol 48: 275-289

Kokelaar BP, Durant GP (1983) The submarine eruption and erosion of Surtla (Surtsey), Island. J Volcanol Geotherm Res 19: 239-246

Larsen JF (2003) The ~12,000 yBP Okmok I caldera-forming eruption: Snow, ice, and pyroclastic flows. 54th Arctic Science Conference: Extreme Events, Understanding Perturbations to the Physical and Biological Environment, Sept. 22-24, 2003

Larsen JF, Nye C (2003) Petrology and geochemistry of the 2050 yBP Okmok caldera-forming eruption: Origin of the voluminous basaltic-andesite pyroclastic deposits. Bull Volcanol, in review

Lescinsky DT, Fink JH (2000) Lava and ice interaction at stratovolcanoes: Use of characteristic features to determine past glacial extents and future volcanic hazards. J Geophys Res 105(B10): 23,711-23,726

Lorenz V (1986) On the growth of maars and diatremes and its relevance to the formation of tuff rings. Bull Volcanol 48: 265-274

Mann D, Freymueller J, Lu Z (2002) Deformation associated with the 1997 eruption of Okmok volcano, Alaska. J Geophys Res 108(B2), 2108, doi:10.1029/2002JB001925

Miller TP, McGimsey RG, Richter DH, Riehle JR, Nye CJ, Yount ME, Dumoulin JA (1998) Catalog of the historically active volcanoes of Alaska. U.S. Geological Survey Open File Report 98-582, pp 104

Morrissey M, Zimanowski B, Wholetz K, Buettner R (2000) Phreatomagmatic fragmentation. In: Haraldur Sigurdsson (ed) Encyclopedia of Volcanoes. Academic Press, San Diego, 431-445

Neal CA, Begét J, Grey D, Wolfe B (2003) The 1817 eruption of Okmok Caldera, Umnak Island, Alaska: new insights into a complex historical eruption in the eastern Aleutians. EOS Trans. AGU Fall Meeting, in press

Orton GJ (1996) Volcanic environments. In Reading HG (ed) Sedimentary Environments: Processes, Facies & Stratigraphy. Blackwell Science, Oxford, 485-567

Post A, LaChapelle ER (2000) Glacier Ice. University of Washington Press, Seattle, pp 145

Self S, Kienle J, Huot JP (1980) Ukinrek Maars, Alaska, II. Deposits and formation of the 1977 craters. J Volcanol Geothermal Res 7: 39-65

Skilling IP (2002) Basaltic pahoehoe lava-fed deltas: large-scale characteristics, clast generation, emplacement processes and environmental discrimination. In Smellie JL and Chapman MG (eds) Volcano-Ice Interaction on Earth and Mars. Geological Society, London, Special Publications 202: 91-113

Thorarinsson S (1964) Surtsey, the new island in the North Atlantic. Almenna Bokafelagid, Reykjavik, pp 63

Waters AC, Fisher RV (1971) Base surges and their deposits: Capelinhos and Ta'al Volcanoes. J Geophys Res 76(23): 5596-5614

White JDL (1996) Pre-emergent construction of a lacustrine basaltic volcano, Pahvant Butte, Utah (USA). Bull Volcanol 58: 249-262

White JDL (2001) Eruption and reshaping of Pahvant Butte Volcano in Pleistocene Lake Bonneville. In: Volcaniclastic Sedimentation in Lacustrine Settings. White JDL and Riggs NR (eds) Spec Publs int Assoc Sediment 30: 61-80. Blackwell Science, Oxford

White JDL, Houghton B (2000) Surtseyan and related phreatomagmatic eruptions. In: Haraldur Sigurdsson (ed) Encyclopedia of Volcanoes. Academic Press, San Diego

Wilson L (1980) Relationships between pressure, volatile content and ejecta velocity in three types of volcanic explosions. J Volcanol and Geotherm Res 8: 297-313

Wohletz KH (1986) Explosive magma-water interactions: Thermodynamics, explosive mechanisms, and field studies. Bull Volcanol 48: 245-264

Wohletz KH, Sheridan MF (1983) Hydrovolcanic explosions II: Evolution of basaltic tuff rings and tuff cones. American Journal of Science 283: 385-41

Wolfe BA (2001) Paleohydrology of a catastrophic flood release from Okmok Caldera and post-flood eruption history at Okmok Volcano, Umnak Island, Alaska. Unpubl MSc thesis, University of Alaska Fairbanks, pp 100

Wolfe BA, Begét JE (2002) Destruction of an Aleut village by a catastrophic flood release from Okmok Caldera, Umnak Island, Alaska. GSA Abstracts with Programs 34(6)

Wolfe BA, Begét JE (2003) Hydrologic hazards from catastrophic caldera dam failures: examples from Okmok Caldera, Umnak Island, Alaska. Geology, in press

Wong LJ (2002) Intra-caldera events: A look at the hydrovolcanic deposit stratigraphically located between two caldera-forming eruptions of Okmok Volcano, Umnak Island, Alaska. EOS Trans. AGU 83(47) Fall Meet. Suppl., Abstract V11A-1378

Appendix A - Detailed map and stratigraphy of Cone D

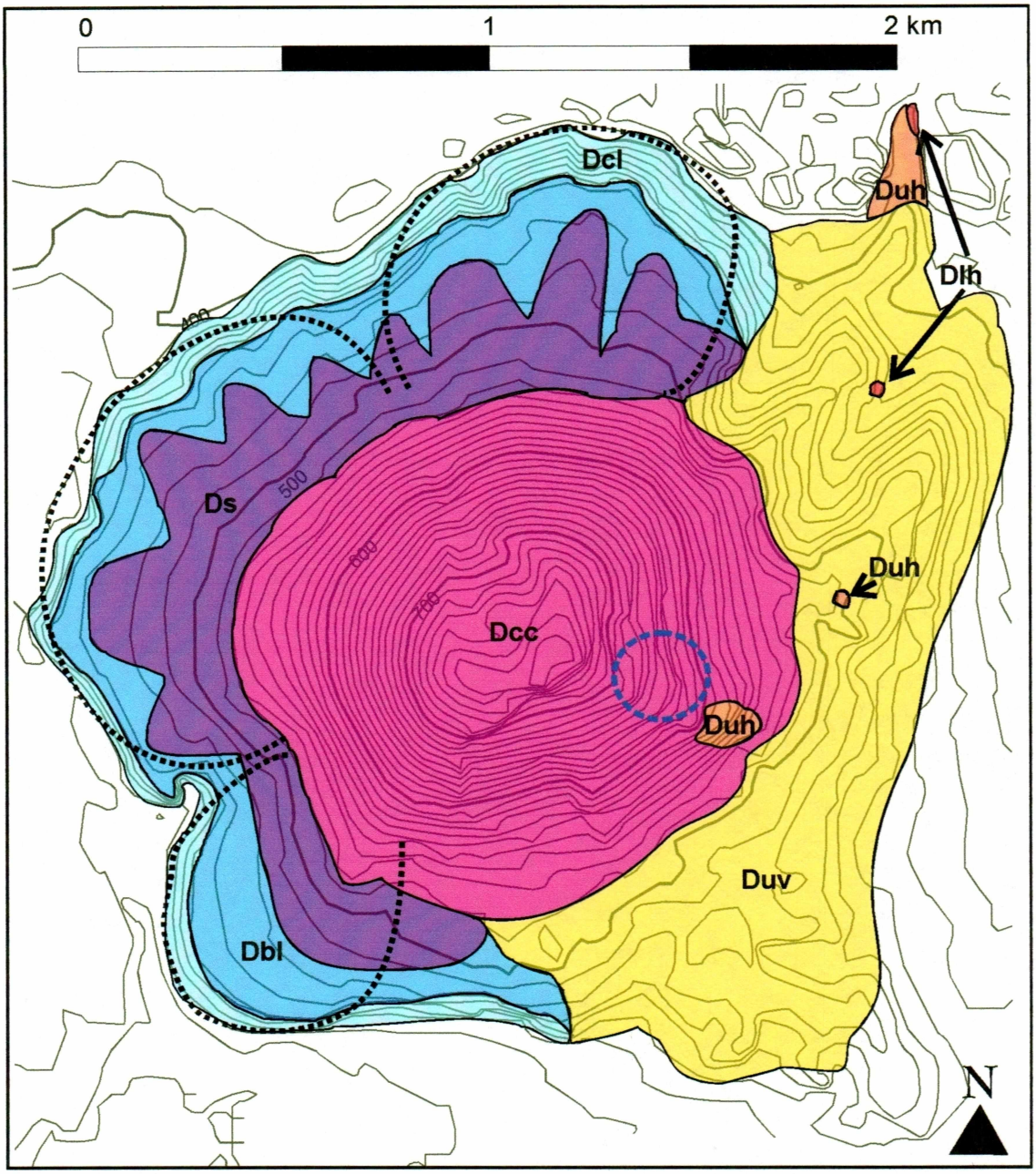

Ds	Surge Deposits	Dcl	Cone D Cliff Lavas
Dl	Lacustrine Deposits*	Duv	Unconsolidated Volcaniclastics
Dcc	Cone D Cinders	Duh	Cone D Upper Hyalotuff
Dbl	Cone D Bench Lavas	Dlh	Cone D Lower Hyalotuff

*Deposits from unit Dl are overlain by Ds deposits and do not appear in map view